Isovalent-substitution effect on the Verwey-type transition in the *A*-site-ordered double perovskite $(Ba,Sr)RFe_2O_5$

J. Nakamura,[1] M. Karppinen,[1,*] P. Karen,[2] J. Lindén,[3] and H. Yamauchi[1]
[1]*Materials and Structures Laboratory, Tokyo Institute of Technology, Yokohama 226-8503, Japan*
[2]*Department of Chemistry, University of Oslo, N-0315 Oslo, Norway*
[3]*Department of Physics, Åbo Akademi, FIN-20500 Turku, Finland*
(Received 24 February 2004; revised manuscript received 17 July 2004; published 8 October 2004)

Two types of chemical-pressure effects on the Verwey-type transition in $BaSmFe_2O_5$ are studied, viz., ionic-size contractions at the Ba and Sm sites. Whereas the replacement of Sm by the smaller Eu and Gd atoms increases the transition temperature T_V from 232 K to 264 K, the Sr-for-Ba substitution decreases it from 232 K to 180 K for $x=0.15$ in $(Ba_{1-x}Sr_x)SmFe_2O_5$. Of various structural parameters determined by synchrotron x-ray diffraction above T_V, the magnitude of the orthorhombic distortion ($=b-a$) is found to correlate with T_V in a manner that unifies both substitution schemes. It is suggested that when an increase in $b-a$ above T_V is achieved by means of the structural substitution, it makes it easier for the d_{xz} Fe^{2+} orbital ordering to occur below T_V.

DOI: 10.1103/PhysRevB.70.144104 PACS number(s): 61.50.Ks, 61.10.−i

I. INTRODUCTION

The *A*-site ordered double-perovskite phase $AA'B_2O_{5+\delta}$ with the *B*-site occupied solely by iron was reported[1] for $A=Ba$ and $A'=Sm,Nd$ in 1999. At $\delta=0$, the $BaRFe_2O_{5+\delta}$ structure consists of repeated slabs of double-layered square pyramids, $(FeO_{5/2})_{2n}$, filled with Ba and separated by the rare-earth-metal atom *R*. From ^{57}Fe Mössbauer spectroscopy, a valence mixing akin to the Verwey transition in magnetite (Fe_3O_4) was revealed via observation of Fe^{2+} and Fe^{3+} states below the transition temperature T_V and $Fe^{2.5+}$ above T_V.[2] The transition is accompanied by abrupt changes in volume, entropy, and electrical conductivity and by the appearance of a small magnetoresistance effect.[3–5]

Above the T_V of 200–300 K (T_V depending on *R*), the pseudotetragonal $BaRFe_2O_5$ experiences a slight orthorhombic distortion that eventually vanishes at the Néel temperature T_N of ~430 K (independent of *R*).[6] Below T_V, a three-dimensional charge ordering occurs. The resulting structure has alternating chains of Fe^{2+} and Fe^{3+},[3,7,8] and exhibits an increased orthorhombic distortion that implies ordering of the doubly occupied d_{xz} orbitals of Fe^{2+}.[6,9] This in turn explains why the charge-ordering pattern is not of the checkerboard arrangement that would minimize Coulombic repulsion if point charges only were considered. Variation of T_V as a function of *R* in $BaRFe_2O_5$,[4,6] shows that the charge and orbital ordering is most stable when *R* is small. The highest T_V of 309 K is accordingly registered for $R=Y$.[9] This favorable effect of small *R* on the stability of the charge-ordered phase is interpreted in terms of diminishing interference of the "hard" *R* atoms with the large orthorhombic distortion that accommodates the d_{xz} orbital ordering (in contrast to the behavior of the "soft" Ba atom).[4]

The stability of the charge ordering decreases also with a departure from the ideal ratio of the two integer iron valences. Such an imbalance can either be induced by the added oxygen δ, or by substituting the trivalent *R* with a divalent element such as Ca. Both are shown to depress T_V, but in a different manner.[7,10] This suggests the existence of a contribution from the *chemical pressure* (an atomic-size difference) for the case of Ca substitution. From a study on the *physical-pressure* effect on $BaSmFe_2O_5$ it was learned that T_V decreases with increasing hydrostatic pressure at a rate of approximately 57 K/GPa.[11]

In the present article, we show that the Verwey-type transition in $(Ba,Sr)RFe_2O_5$ is affected differently by chemical-pressure effects at the two *A*-cation sites, viz., *R* and Ba. In order to do so, two substitution series of the $BaSmFe_2O_5$ parent phase are synthesized and investigated: $BaRFe_2O_{5+\delta}$ ($R=Sm,Eu,Gd$) and $(Ba_{1-x}Sr_x)SmFe_2O_{5+\delta}$ ($0\leqslant x\leqslant 0.15$).

II. EXPERIMENT

Syntheses and oxygen-content characterization. The polycrystalline samples were synthesized from high-purity $BaCO_3$, $SrCO_3$, R_2O_3, and Fe_2O_3/Fe, using two methods. The first was a ceramic synthesis followed by an oxygen-content control by Fe getter and tempering in 5% H_2/Ar ($R=Sm,Eu$; see Ref. 12 for details). The second was a citrate nanoprecursor method, followed by equilibration and quenching ($R=Gd$; see Ref. 8 for details). For determination of the oxygen nonstoichiometry δ, powdered samples were digested in 6M HCl, and the resulting solution was titrated with cerium(IV)nitrate of precise molarity, under Ar protective atmosphere. We aimed to maintain δ constant throughout the sample series; the result is contained in the interval of $0.019(5)\leqslant\delta\leqslant 0.042(5)$. From data in Ref. 4, $\Delta T_V/\Delta\delta=-450(90)$ K can be evaluated for the relevant nonstoichiometry range of $BaRFe_2O_{5+\delta}$. Using this value, a change in T_V caused by δ not being constant can be calculated, giving 9(2) K across the nonstoichiometry interval of the *R*-substitution series and 6(2) K for the Sr-for-Ba substitution series.

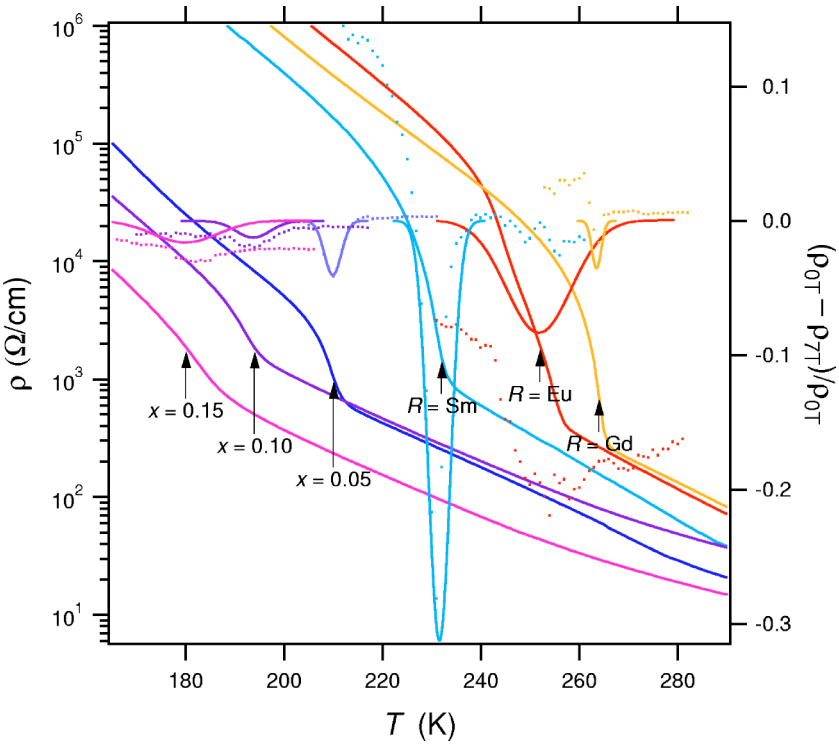

FIG. 1. (Color online) Resistivities ρ_{0T} at zero field (full lines) and the magnetoresistancelike values $(\rho_{0T}-\rho_{7T})/\rho_{0T}$ (dots) for $BaRFe_2O_5$ and $(Ba_{1-x}Sr_x)SmFe_2O_5$. The fitted Gaussian peaks related to magnetoresistance are drawn as a full line, and the position of their tops (T_V) is marked by the tags of the resistivity curves.

Transition temperatures. Resistivities of the sintered samples were measured by a four-point method (a Quantum Design PPMS-9 instrument) as a function of temperature under magnetic field of 0 and 7 T. A magnetoresistancelike curve was obtained as the relative difference of these two series, and the peaks on this difference curve occurring at the Verwey transition were extracted by least-squares fitting as Gaussian curves on a fourth-order polynomial background. The peak top was regarded to be the transition temperature T_V. Figure 1 illustrates this procedure.

Structural parameters. Synchrotron x-ray powder diffraction (SXPD) patterns were collected at the BL02B2 beamline of SPring-8, Japan, with radiation of the wavelength $\lambda = 0.50075$ Å for 5–15 min on each sample sealed in a quartz capillary of 0.1 mm in diameter. An interval between 6° and 40° in 2θ of the imaging-plate detector was scanned for use in Rietveld refinements by the RIETAN-2000 program.[13]

III. RESULTS AND DISCUSSION

In Fig. 2, the effect of ionic radius[14] on the determined T_V is compared for the substitutions at the *R* and Ba sites. It is seen that whereas decreasing ionic radius at the (Ba,Sr) site decreases T_V, decreasing the size of the *R* atom does the opposite. In order to explain this behavior in terms of steric arguments, interatomic distances for the two substitution series were evaluated at a reference temperature of 300 K ($T > T_V$) (from the refined crystal-structure data listed in Tables I and II) for $BaRFe_2O_{5+\delta}$ and $(Ba_{1-x}Sr_x)SmFe_2O_{5+\delta}$. With allowances for somewhat different oxygen contents, these data are consistent with the earlier published data for the $BaRFe_2O_{5+\delta}$ phases.[1,8,10]

It is seen from Tables I and II that the variations in lattice parameters show a marked difference between the two types of chemical pressure. That is, whereas the contraction of the ionic size at the *R* site shortens equally *a*, *b*, and *c*, the contraction in the ionic size at the Ba site leaves *c* unchanged and decreases only the longer one of the orthorhombic (*a* and *b*) parameters. In order to explain this observation, we need to note two important differences between these two sites in the parent phase $BaSmFe_2O_5$: (1) in terms of bond

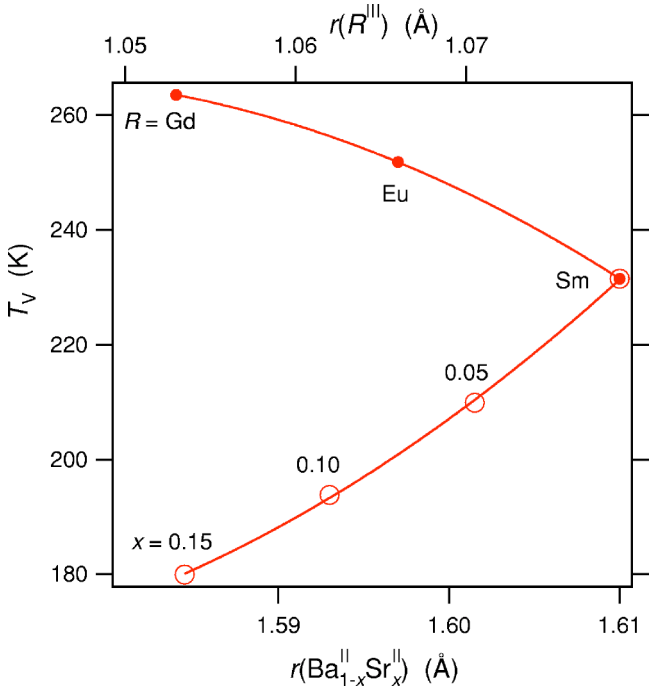

FIG. 2. (Color online) T_V vs the Shannon "IR" ionic radius (Ref. 14) *r*, at the *R* site and the (Ba,Sr) site in $BaRFe_2O_5$ and $(Ba_{1-x}Sr_x)SmFe_2O_5$.

TABLE I. SXPD refinement results for $BaRFe_2O_{5+\delta}$ (R=Gd,Eu,Sm) samples at 300 K. Space group *Pmmm* (No. 47): R at (0,0,1/2), Ba at (0,0,0), Fe at (1/2,1/2,z), O(1) at (1/2,1/2,0), O(2) at (1/2,0,z), O(3) at (0,1/2,z), O(4)$\equiv\delta$ at (1/2,1/2,1/2). The occupancy of O(4) was fixed to cerimetric δ. Isotropic atomic displacement parameters B were constrained equal for all oxygens. R_e is the minimum weighted-profile (R_{wp}) value expected statistically.

	R	Gd	Eu	Sm
	T_V (K)	264	252	232
	Cerimetric δ	0.019	0.035	0.039
Unit cell	a (Å)	3.9313(3)	3.9368(2)	3.9413(2)
	b (Å)	3.9537(3)	3.9578(2)	3.9597(2)
	c (Å)	7.5942(5)	7.5995(4)	7.6105(4)
	$b-a$ (Å)	0.0224(6)	0.0210(4)	0.0184(4)
R	B (Å^2)	0.68(5)	0.75(5)	0.63(6)
Ba	B (Å^2)	0.44(5)	0.40(6)	0.49(6)
Fe	z	0.2637(4)	0.2637(4)	0.2629(5)
	B (Å^2)	0.50(4)	0.56(4)	0.40(4)
O(1)	B (Å^2)	0.77(12)	1.02(13)	0.78(14)
O(2)	z	0.3059(21)	0.3183(20)	0.3206(23)
O(3)	z	0.3129(21)	0.3018(20)	0.2977(23)
R_{wp}		9.52	6.39	6.87
R_e		2.53	2.55	2.41
Bond lengths	Fe–O(1)	2.0028(33)	2.0044(35)	2.0011(38)
	Fe–O(2)	2.0027(26)	2.0220(34)	2.0280(40)
	Fe–O(3)	2.0009(30)	1.9896(23)	1.9883(24)
	Fe–O(4)	1.7943(33)	1.7954(35)	1.8041(38)
	Ba–O(1)	2.7878(1)	2.7912(1)	2.7935(1)
	Ba–O(2)	3.0431(121)	3.1192(122)	3.1365(136)
	Ba–O(3)	3.0915(122)	3.0296(119)	3.0088(131)
	R–O(2)	2.4570(95)	2.4040(90)	2.3973(10)
	R–O(3)	2.4342(92)	2.4867(95)	2.5081(107)
	R–O(4)	2.7878(1)	2.7912(1)	2.7935(1)

valence, the Sm site is underbonded whereas the Ba site is not,[1] and (2) the R atom is harder, less polarizable, and less deformable than Ba. Consequently, the decreasing size of R should contract the coordination cube RO_8 along all three directions in order to maintain the highest bond-valence sum. When the ionic size at the Ba site is decreased, the resulting underbonding is less severe and more efficiently eliminated by contraction within the (ab) plane as there is no Ba–O bond parallel with c. The fact that, in the end, only the b parameter is contracted must be associated with the high hardness of the R atom, which becomes more exposed as the diminishing ionic size at the Ba site "deflates" the structure. Accordingly, the orthorhombic distortion, as simply represented by the difference $b-a$, decreases with increasing Sr substitution level x (Table II). While the orthorhombic distortion decreases with increasing Sr substitution level at the Ba site as one means of chemical pressure, it increases when the unit-cell volume is suppressed by replacing the larger R by a smaller R as the other means of chemical pressure. The common denominator of this behavior is the higher hardness of the R atom than that of the Ba atom, which allows the orthorhombic distortion to increase when R becomes smaller, but suppresses it when the ionic size at the Ba site decreases for a given R.

In Fig. 3 all the T_V values that were determined in this study are plotted against lattice parameters a, b, and c, the unit-cell volume V, and the orthorhombic distortion, $b-a$. Only $b-a$ provides a correlation with T_V that is common for both substitution schemes. The occurrence of this correlation reflects an increasing stability of the charge-ordered phase (increasing T_V) via improving steric conditions for the d_{xz} Fe^{2+} orbital ordering. In a parallel application of the LeChatelier principle, we note that compression of the lattice by means of physical pressure decreases T_V (Ref. 11) because V is increasing at the transition into the low-temperature orbital-ordered state. Thus it is not surprising to observe that the orthorhombic distortion decreases under increasing hydrostatic pressure.[11]

Further analysis was carried out based on the refined structure data, in order to see other structural parameters that may correlate with T_V. The chosen parameters are illustrated in Fig. 4: the Fe–Fe distance across the R layer (L_1), the distance between the in-plane Fe atoms (L_2; along both a and b), the Fe–Fe distance across the BaO layer (L_3), and the

TABLE II. SXPD refinement results for $(Ba_{1-x}Sr_x)SmFe_2O_{5+\delta}$ ($x=0, 0.05, 0.10, 0.15$) samples at 300 K. (See Table I caption for details.)

	x	0.0	0.05	0.10	0.15
	T_V (K)	232	210	194	180
	Cerimetric δ	0.039	0.041	0.042	0.029
Unit cell	a (Å)	3.9413(2)	3.9424(2)	3.9420(3)	3.9433(1)
	b (Å)	3.9597(2)	3.9567(2)	3.9534(3)	3.9528(1)
	c (Å)	7.6105(4)	7.6112(4)	7.6139(6)	7.6091(2)
	$b-a$ (Å)	0.0184(4)	0.0143(4)	0.0114(6)	0.0095(2)
Sm	B (Å^2)	0.63(6)	0.62(4)	0.72(5)	0.77(3)
Ba/Sr	B (Å^2)	0.49(6)	0.52(4)	0.48(5)	0.33(4)
Fe	z	0.2629(5)	0.2621(4)	0.2621(4)	0.2622(3)
	B (Å^2)	0.40(4)	0.53(3)	0.47(4)	0.40(3)
O(1)	B (Å^2)	0.78(14)	0.84(11)	1.05(12)	0.95(9)
O(2)	z	0.3206(23)	0.3091(23)	0.3030(36)	0.2982(23)
O(3)	z	0.2977(23)	0.3043(23)	0.3083(36)	0.3150(24)
R_{wp}		6.87	9.12	9.47	6.63
R_e		2.41	3.79	4.19	2.99
Bond lengths	Fe–O(1)	2.0011(38)	1.9955(28)	1.9956(33)	1.9952(22)
	Fe–O(2)	2.0280(40)	2.0104(31)	2.0011(44)	1.9953(25)
	Fe–O(3)	1.9883(24)	1.9971(28)	2.0022(49)	2.0123(36)
	Fe–O(4)	1.8041(38)	1.8101(28)	1.8113(33)	1.8093(22)
	Ba/Sr–O(1)	2.7935(1)	2.7928(1)	2.7915(1)	2.7917(1)
	Ba/Sr–O(2)	3.1365(136)	3.0695(132)	3.0345(211)	3.0061(135)
	Ba/Sr–O(3)	3.0088(131)	3.0460(130)	3.0692(211)	3.1070(138)
	Sm–O(2)	2.3973(10)	2.4487(102)	2.4768(168)	2.4989(110)
	Sm–O(3)	2.5081(107)	2.4764(103)	2.4570(164)	2.4262(104)
	Sm–O(4)	2.7935(1)	2.7928(1)	2.7915(1)	2.7917(1)

buckling angle of the FeO_2 plane (ε; along both a and b). Figure 5 shows how these parameters correlate with T_V. It is seen that there is no correlation common to both types of the isovalent substitutions investigated in this study. Individually, the T_V values for the R-substitution series correlate with distances along c, in particular with L_1, and this is directly related to the ionic size of R as discussed above. The values of T_V for the Sr-for-Ba substitution series correlate accordingly with distances in the (ab) plane. As a function of the diminishing ionic size at the Ba site (which causes a decrease in T_V), $L_2(b)$ changes more profoundly than $L_2(a)$, as follows from the predominant contraction along b as a function of the increasing substitution level x. Interestingly, the buckling angle $\varepsilon(b)$ does not become sharper as b contracts. The angle actually becomes more open as a function of increasing x, because the angle apex O(2) moves towards the center of the

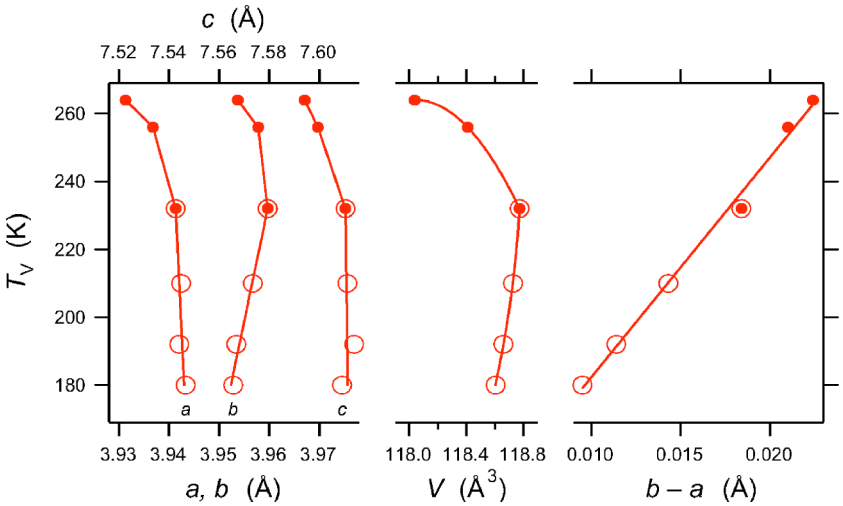

FIG. 3. (Color online) T_V vs lattice parameters a, b, and c, unit-cell volume V, and the orthorhombic distortion $b-a$ for $BaRFe_2O_5$ (solid circles) and $(Ba_{1-x}Sr_x)SmFe_2O_5$ (open circles; hence a double symbol for the parent phase). The size of the symbols is several times larger than standard deviations.

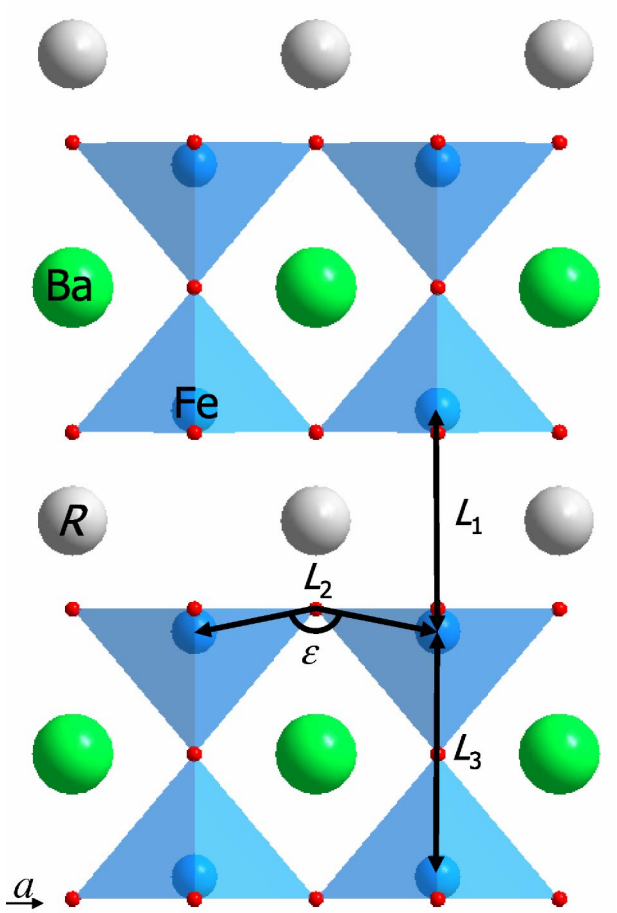

FIG. 4. (Color online) A schematic illustration of the BaRFe$_2$O$_5$ structure in the valence-mixed state. Iron–(oxygen)–iron distances L_1, L_2, L_3 and the buckling angle ε of the FeO$_2$ plane are marked.

iron-oxygen slab. The apex O(3) of the angle $\varepsilon(a)$, which is along the shorter of the orthorhombic axes, does the opposite, and the angle becomes sharper even though the unit-cell parameter a is not changing. The process behind this can be followed from bond distances in Table II and understood by recollecting that Sm is slightly underbonded in terms of bond valence, whereas Ba is not.[1] According to the bond-valence distortion theorem,[15] the Sm coordination cube is distorted in order to keep the Sm bond-valence sum up. When the diminishing ionic size at the Ba site deflates the structure, the Sm underbonding, as well as the distortion of its coordination, decreases alongside. However, a further Sr-for-Ba substitution eventually produces a need for a further distortion of the Ba/Sr coordination so that the bond-valence sum is maintained. There appears to be no other correlation revealed by inspection of the individual bond distances than such bond-valence effects and the already identified change in the orthorhombic distortion.

IV. CONCLUSIONS

Chemical-pressure effects were evaluated through two independent isovalent substitution schemes, viz., Sr-for-Ba substitution in (Ba$_{1-x}$Sr$_x$)SmFe$_2$O$_5$ and decrease in the R ionic size in BaRFe$_2$O$_5$. The results show that the Verwey-type transition is affected according to a single criterion of how far the induced steric changes above T_V resemble those needed to accommodate the d_{xz} orbital ordering of Fe^{2+} below T_V. Because the d_{xz} ordering proceeds upon an increase in orthorhombic distortion, T_V as a measure of stability of the charge-ordered state increases with increasing orthorhombic distortion in the valence mixed state (distortion evaluated at 300 K). The local chemical-pressure contractions exerted by the two substitution schemes correlate in terms of T_V with the previously studied[11] hydrostatic compressions only via the linkage between orbital ordering and orthorhombic distortion. This once again proves that the so-called chemical pressure is not the same as the physical pressure when exerted on structures exhibiting anisotropy of the bond network. Therefore, chemical-pressure substitutions in such structures are important means to control and tune the electronic properties.

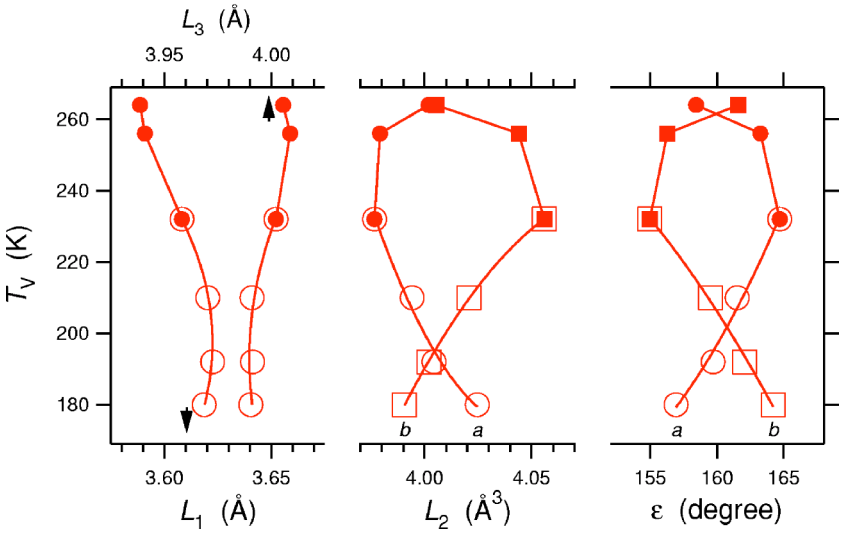

FIG. 5. (Color online) T_V vs Fe–(O)–Fe distances L_1, L_2, and L_3, and the Fe–O–Fe buckling angle ε (Fig. 4; note that L_2 and ε are considered separately along a and b), for BaRFe$_2$O$_5$ (solid symbols) and (Ba$_{1-x}$Sr$_x$)SmFe$_2$O$_5$ (open symbols; hence a double symbol for the parent phase). The size of symbols is comparable with standard deviations.

ACKNOWLEDGMENTS

This work was supported by Grants-in-aid for Scientific Research (Nos. 15206002 and 15206071) from the Japan Society for the Promotion of Science. The synchrotron radiation experiments were performed under the auspices of SPring-8 (PRC No. 2002B0170). Professor Satoshi Sasaki and Dr. Ken-ichi Kato and Dr. Kouji Yamawaki are thanked for their experimental guidance.

---

*Author to whom correspondence should be addressed. Electronic address: karppinen@msl.titech.ac.jp

[1] P. Karen and P.M. Woodward, J. Mater. Chem. **9**, 789 (1999).
[2] J. Lindén, P. Karen, A. Kjekshus, J. Miettinen, T. Pietari, and M. Karppinen, Phys. Rev. B **60**, 15251 (1999).
[3] P. Karen, P. Woodward, J. Lindén, T. Vogt, A. Studer, and P. Fischer, Phys. Rev. B **64**, 214405 (2001).
[4] P. Karen, J. Solid State Chem. **177**, 281 (2004).
[5] J. Nakamura, J. Lindén, M. Karppinen, and H. Yamauchi, Appl. Phys. Lett. **77**, 1683 (2000).
[6] P.M. Woodward, E. Suard, and P. Karen, J. Am. Chem. Soc. **125**, 8889 (2003).
[7] P. Karen, P.M. Woodward, P.N. Santhosh, T. Vogt, P.W. Stephens, and S. Pagola, J. Solid State Chem. **167**, 480 (2002).
[8] P. Karen, J. Solid State Chem. **170**, 9 (2003).
[9] P.M. Woodward and P. Karen, Inorg. Chem. **42**, 1121 (2003).
[10] J. Nakamura, J. Lindén, H. Yamauchi, and M. Karppinen, Solid State Commun. **121**, 269 (2002).
[11] Y. Moritomo, M. Hanawa, Y. Ohishi, K. Kato, J. Nakamura, M. Karppinen, and H. Yamauchi, Phys. Rev. B **68**, 060101 (2003).
[12] J. Nakamura, J. Lindén, H. Suematsu, M. Karppinen, and H. Yamauchi, Physica C **338**, 121 (2000).
[13] F. Izumi and T. Ikeda, Mater. Sci. Forum **321**, 198 (2000).
[14] R.D. Shannon, Acta Crystallogr., Sect. A: Cryst. Phys., Diffr., Theor. Gen. Crystallogr. **32**, 751 (1976).
[15] I.D. Brown, *The Chemical Bond in Inorganic Chemistry: The Bond Valence Model* (Oxford University Press, New York, 2002), p. 33.